



## Sonar image segmentation based on GMRF and level-set models

Xiu-Fen Ye<sup>a,\*</sup>, Zhe-Hui Zhang<sup>a</sup>, Peter X. Liu<sup>b</sup>, Hong-Ling Guan<sup>a</sup>

<sup>a</sup> College of Automation, Harbin Engineering University, Harbin, Heilongjiang 150001, PR China

<sup>b</sup> Department of Systems and Computer Engineering, Carleton University, Ottawa, ON, Canada K1S 5B6

### ARTICLE INFO

#### Article history:

Received 13 May 2009

Accepted 1 March 2010

Available online 16 March 2010

#### Keywords:

Sonar image

GMRF

Level set

Segmentation

### ABSTRACT

We propose two new level-set models to address the segmentation problem in sonar images. Local texture features, extracted using the Gauss–Markov random field model, are integrated into level-set energy functions to dynamically select regions of interest. Then, new two-phase level-set and multiphase level-set models are obtained by minimizing each new energy function, and the selection of model parameters is analyzed. The proposed models do not require re-initialization, which is usually a very costly procedure. Segmentation experiments on both synthetic and real sonar images show that the proposed two level-set models are accurate and robust when they are applied to noisy sonar images.

© 2010 Elsevier Ltd. All rights reserved.

## 1. Introduction

Three types of regions usually have to be identified in high-resolution sonar images: highlight, shadow, and sea-bottom reverberation. The highlight area originates from acoustic wave reflection from an object, whereas the shadow zone comes from a lack of acoustic reverberation behind the object. The remaining information consists of so-called sea-bottom reverberation (Mignotte and Collet, 1999; Mignotte et al., 2000; Schmitt et al., 1996). The region of interest is usually the highlight or shadow area because the highlight features are generally less discriminative than the shadow shapes for the classification of objects lying on the seabed. The third region in sonar images, sea-bottom reverberation, is more difficult to differentiate in that it contains a large amount of speckle noise. The gray values associated with some substances, such as rocks, animals, and impurities, are close to those of the highlight and shadow regions. Sonar images are notorious for speckle noise and low signal-to-noise ratios and hence are very difficult to segment.

A Markovian segmentation algorithm was used by Mignotte and Collet (1999) for three-class sonar image segmentation. Later, they developed a hierarchical Markov random field model for two-class sonar image segmentation (Mignotte et al. 2000). Although their results were satisfactory, the processing procedures are quite complicated and computationally costly. A statistical snake method used to extract the contours of mine-like objects was implemented by Reed et al. (2003). For this method, prior information is used to detect the mine-like objects

with the Markov model and to restrict the movement of the snakes.

The level-set method was introduced by Osher and Sethian (1988). Later, Chan and Vese (2001) proposed active contours without edges using a reducing Mumford–Shah function (Mumford and Shah, 1989). In 2002, Vese and Chan (2002) developed a multiphase segmentation model (also see Brox and Weickert, 2006; Chung and Vese, 2005; Mansouri et al., 2006). The key idea was to minimize the energy with the local mean, thereby driving the zero level set to the edges of the objects. Although their method is promising, the models are not suitable or effective for segmenting sonar images in the presence of speckle noise. Active contours and level-set methods were applied to the segmentation of areas like the seabed (Lianantonakis and Petillot, 2005a, 2007). In this case, global texture features were extracted from a side scan image containing two distinct regions. The Haralick feature set based on a co-occurrence matrix was considered and yielded high-quality segmentation of seabed areas.

In this paper, we consider different segmentation tasks. First, the local texture features of sonar images are extracted based on the Gauss–Markov random field (GMRF) model and integrated into the level-set energy functions. Then, the level-set evolution function is obtained by minimizing the energy. Finally, experimental results for both synthetic and real sonar images are presented and discussed.

After this introduction, Section 2 briefly introduces Chan–Vese two-phase and multiphase models; Section 3 describes the GMRF model; Section 4 proposes new level-set models; Section 5 presents sonar image segmentation results for both synthetic and real images; and the paper is concluded and some remarks are given in Section 6.

\* Corresponding author.

E-mail address: [xexifuren@hrbeu.edu.cn](mailto:xexifuren@hrbeu.edu.cn) (X.-F. Ye).

## 2. Chan–Vese active contour models

### 2.1. The two-phase model

For the two-phase model, it is assumed that the image  $u_0$  is formed by two regions of approximately piecewise-constant intensities. Let  $\text{inside}(C)$  denote the variable inside contour  $C$  and  $\text{outside}(C)$  denote the variable outside contour  $C$ . Consider the following “fitting energy”:

$$E(C, c_1, c_2) = \iint_{\text{inside}(C)} |u_0 - c_1|^2 dx dy + \iint_{\text{outside}(C)} |u_0 - c_2|^2 dx dy \quad (1)$$

where  $c_1$  and  $c_2$  are the average intensities of  $u_0$  inside and outside  $C$ , respectively. It is clear that the “fitting energy” is minimized when  $C$  corresponds to the boundary of the objects (Chan and Vese, 2001).

The addition of regularizing terms into Eq. (1), leaves the energy defined for  $\mu \geq 0$ ,  $v \geq 0$ , and the fixed parameters  $\lambda_1, \lambda_2 > 0$

$$E(C, c_1, c_2) = \mu \cdot \text{length}(C) + v \cdot \text{area}(\text{inside}(C)) + \lambda_1 \iint_{\text{inside}(C)} |u_0 - c_1|^2 dx dy + \lambda_2 \iint_{\text{outside}(C)} |u_0 - c_2|^2 dx dy \quad (2)$$

where  $\text{length}(C)$  denotes the length of contour  $C$  and  $\text{area}(\text{inside}(C))$  denotes the area inside contour  $C$ .

The space variable is denoted by  $(x, y) \in \Omega \subset \mathbb{R}^2$ . The level-set evolution function is obtained through minimizing Eq. (2) by evaluating the Euler–Lagrange equations

$$\frac{\partial \phi}{\partial t} = \delta_\varepsilon(\phi) \left[ \mu \cdot \text{div} \left( \frac{\nabla \phi}{|\nabla \phi|} \right) - v - \lambda_1 (u_0 - c_1)^2 + \lambda_2 (u_0 - c_2)^2 \right] \quad (3)$$

where  $C$  is represented by the zero level set of a signed distance function (SDF)  $\phi$ , and  $\text{div}$  is the divergence.

### 2.2. The multiphase model for piecewise-constant segmentation

>Vese and Chan generalized their two-phase model of piecewise-constant segmentation of images with more than two regions. Consider  $n$  level-set functions  $\phi_i : \Omega \rightarrow \mathbb{R}$ ,  $i=1, \dots, n$ . To partition the image into  $2^n$  regions, the “fitting energy” is written as

$$E(\phi, c) = \sum_{j=1}^{2^n} \lambda_j \iint_{\Omega} (u_0 - c_j) \chi_j dx dy + \sum_{i=1}^n v \iint_{\Omega} |\nabla H(\phi_i)| dx dy \quad (4)$$

where  $\chi_j$  is the characteristic function for class  $j$ , and  $H$  is the Heaviside function. We can obtain the two-phase energy when  $n=1$ . The energy for four phases or classes (when  $n=2$ , level-set function in Fig. 1) is as follows:

$$E_4(\phi, c) = \iint_{\Omega} (u_0 - c_{11})^2 H(\phi_1) H(\phi_2) dx dy + \iint_{\Omega} (u_0 - c_{10})^2 H(\phi_1) (1 - H(\phi_2)) dx dy + \iint_{\Omega} (u_0 - c_{01})^2 (1 - H(\phi_1)) H(\phi_2) dx dy$$

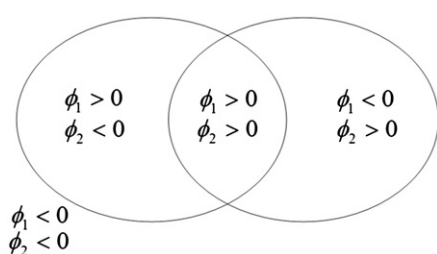


**Fig. 1.** Zero level sets of with four domains partition ( $n=2$ ).

$$+ \iint_{\Omega} (u_0 - c_{00})^2 (1 - H(\phi_1)) (1 - H(\phi_2)) dx dy + v \iint_{\Omega} |\nabla H(\phi_1)| dx dy + v \iint_{\Omega} |\nabla H(\phi_2)| dx dy \quad (5)$$

where  $c_{11}, c_{10}, c_{01}$ , and  $c_{00}$  are local means of each domain in Fig. 1.

Then, the Euler–Lagrange equations obtained by minimizing Eq. (5) are

$$\frac{\partial \phi_1}{\partial t} = \delta_\varepsilon(\phi_1) \left\{ v \cdot \text{div} \left( \frac{\nabla \phi_1}{|\nabla \phi_1|} \right) - [(u_0 - c_{11})^2 - (u_0 - c_{01})^2] H_\varepsilon(\phi_2) + [(u_0 - c_{10})^2 - (u_0 - c_{00})^2] (1 - H_\varepsilon(\phi_2)) \right\} \quad (6)$$

$$\frac{\partial \phi_2}{\partial t} = \delta_\varepsilon(\phi_2) \left\{ v \cdot \text{div} \left( \frac{\nabla \phi_2}{|\nabla \phi_2|} \right) - [(u_0 - c_{11})^2 - (u_0 - c_{01})^2] H_\varepsilon(\phi_1) + [(u_0 - c_{01})^2 - (u_0 - c_{00})^2] (1 - H_\varepsilon(\phi_1)) \right\} \quad (7)$$

In Eqs. (6) and (7),  $H_\varepsilon(\phi)$  and  $\delta_\varepsilon(\phi)$  are the normalization functions defined in Eqs. (8) and (9)

$$H_\varepsilon(\phi) = \frac{1}{2} \left( 1 + \frac{2}{\pi} \arctan \left( \frac{\phi}{\varepsilon} \right) \right) \quad (8)$$

$$\delta_\varepsilon(\phi) = H'_\varepsilon(\phi) = \frac{1}{\pi} \cdot \frac{\varepsilon}{\varepsilon^2 + \phi^2} \quad (9)$$

The main limitation of the Chan–Vese two-phase and multiphase models lies in the fact that they can only discriminate regions that have different mean intensities. That is, when the edge of the highlight is vague or the mean value of the highlight region is similar to that of its surroundings, the Chan–Vese models may not obtain satisfactory segmentation results. Hence, the Chan–Vese models are not suitable for images containing severe noise.

## 3. Application of the GMRF model to local texture features

Texture information is very important in extracting reliable and accurate segmentation maps of sonar images, so a considerable amount of work has been done on texture analysis in the past

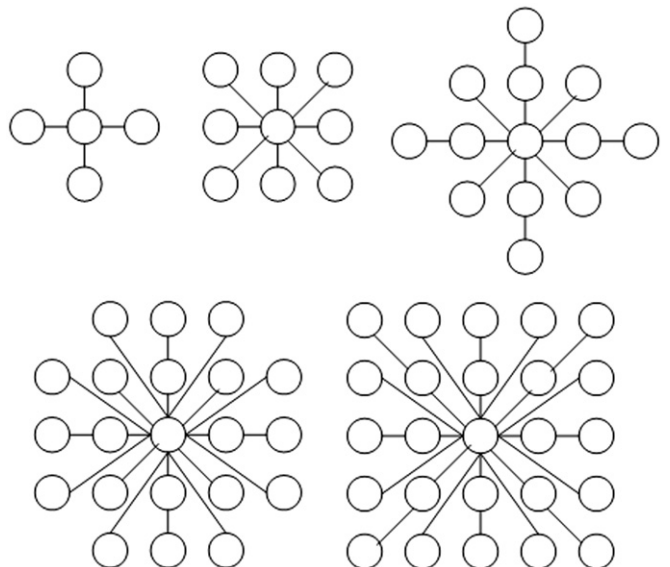


**Fig. 2.** The structure of MRF model for first-order neighbor to fifth-order neighbor.

few decades. Haralick et al. (1973) used a textural feature set for image classification. The Markov random field (MRF) model also shows great potential for representing textures (Krishnamachari and Chellappa, 1997); the MRF model reflects the spatial relationship of the pixels, and its parameters represent the texture elements. In this paper, we employ the MRF model to describe the local texture while considering the relationship of all points in a gray image.

Let  $\Omega \subset \mathbb{R}^2$  denote the image plane, and let  $f : \Omega \times \mathbb{R} \rightarrow \mathbb{R}$  be a given sonar image. Let  $\eta_s$  denote the symmetric neighbor set of site  $s$ . For a discrete label set  $\Omega$ , the probability that the random variable  $f(s)$  takes the value  $f_s$  is denoted  $P(f(s)=f_s)$ , which is abbreviated as  $P(f_s)$ . If the conditional probability  $P(f_s|f(\Omega)) = P(f_s|f(\eta_s)) > 0, \forall s \in \Omega$ ,  $f$  is said to be an MRF on  $\Omega$  with respect to a neighborhood system  $\eta$ , namely,  $P(f_s)$  is only dependent on its neighbors.

The MRF models are described by the conditional probability  $P(f(s)|f(\eta_s^N))$ , where  $s \in \Omega$ , and  $\eta_s^N = \{s+r, r \in \eta^N\}$  is an  $N$ th-order symmetric neighbor set of site  $s$ . The first- to fifth-order neighbor MRF relationships are depicted in Fig. 2. For the first-order case,  $\eta_s^1 = \{s+(0,-1), s+(0,1), s+(-1,0), s+(1,0)\}$ .

$\theta_{11}$	$\theta_9$	$\theta_6$	$\theta_{10}$	$\theta_{12}$
$\theta_7$	$\theta_3$	$\theta_2$	$\theta_4$	$\theta_8$
$\theta_5$	$\theta_1$	$S$	$\theta_1$	$\theta_5$
$\theta_8$	$\theta_4$	$\theta_2$	$\theta_3$	$\theta_7$
$\theta_{12}$	$\theta_{10}$	$\theta_6$	$\theta_9$	$\theta_{11}$

**Fig. 3.** The parameters of MRF model for first-order neighbor to fifth-order neighbor.

If  $f$  is modeled by a GMRF with a symmetric neighborhood  $\eta$ , it can be written as

$$f_s = \sum_{r \in \eta_s} \theta_r f_{s+r} + e_s \quad (10)$$

where  $\theta_r (r \in \eta_s)$  represents the MRF model parameters that characterize the local texture. The parameter set  $\theta$  satisfies Eq. (11)

$$\theta_r = \theta_{-r} \forall r \in \eta_s \quad (11)$$

Fig. 3 shows the MRF model parameters for the first- to fifth-order neighbors of Fig. 2.  $e_s$  is zero-mean Gaussian noise in Eq. (12)

$$e_s = \frac{1}{\sqrt{2\pi\sigma^2}} \exp\left\{-\frac{f_s^2}{2\sigma^2}\right\} \quad (12)$$

Eq. (10) can be also represented by the matrix

$$f_s = \theta^T Q_s + e_s \quad (13)$$

where  $\theta$  is a vector comprised of  $\theta_r$ , and  $Q_s$  is a vector defined by Eq. (14)

$$Q_s = [f_{s+r1} + f_{s-r1}, \dots, f_{s+m} + f_{s-m}]^T \quad (14)$$

Then, the vector  $\theta$  and variance  $\sigma$  can be estimated using the least-square (LSQR) approach presented in Eqs. (15) and (16)

$$\hat{\theta} = \left[ \sum_{s \in \Omega} Q_s Q_s^T \right]^{-1} \left[ \sum_{s \in \Omega} Q_s f_s \right] \quad (15)$$

$$\hat{\sigma} = \frac{1}{M^2} \sum_{s \in \Omega} [f_s - \hat{\theta}^T Q_s] \quad (16)$$

The parameter  $\hat{\theta}$  reflects the local texture feature of the image. Here, we extract local texture features of sonar images using the first- to fifth-order neighbors in the MRF model, as shown in Fig. 2. Fig. 4 shows a real  $132 \times 134$  sonar image and its five texture images based on the different order GMRF neighbors. The corresponding texture-image MRF parameters are presented in Table 1.

To validate the local texture features based on the GMRF model, we extracted the shadow and highlight regions from the

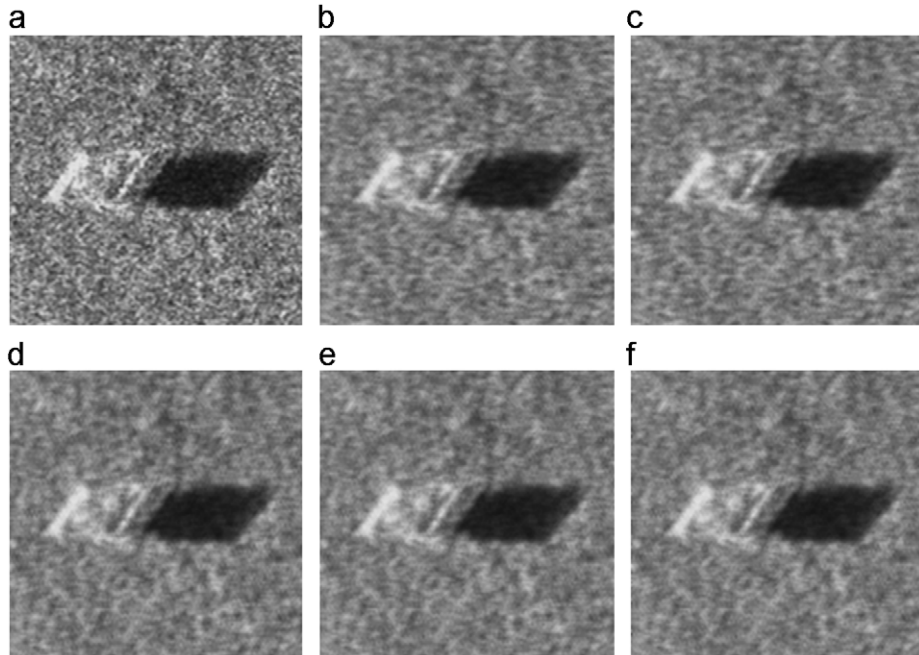


**Fig. 4.** A real sonar image and its texture images based on different orders neighbor of GMRF. (a) Original real sonar image; (b)–(f) are texture images: (b) first-order neighbor; (c) second-order neighbor; (d) third-order neighbor; (e) fourth-order neighbor and (f) fifth-order neighbor.

**Table 1**

The MRF parameters for the texture images in Fig. 3.

	$\theta_1$	$\theta_2$	$\theta_3$	$\theta_4$	$\theta_5$	$\theta_6$	$\theta_7$	$\theta_8$	$\theta_9$	$\theta_{10}$	$\theta_{11}$	$\theta_{12}$
(b)	0.3874	0.1110	—	—	—	—	—	—	—	—	—	—
(c)	0.3718	0.0817	0.0364	0.0090	—	—	—	—	—	—	—	—
(d)	0.3776	0.0673	0.0361	0.0103	-0.0530	0.0606	—	—	—	—	—	—
(e)	0.3717	0.0673	0.0210	-0.0074	-0.0649	0.0379	0.0236	0.0131	0.0083	0.0290	—	—
(f)	0.3703	0.0662	0.0202	-0.0080	-0.0679	0.0392	0.0209	0.0095	0.0021	0.0192	0.0089	0.0189

histograms of the original image and its second-order neighbor image as shown in Figs. 4(a) and (c), respectively. The shadow region is manually selected from the histogram diagram when no noise pixels exist outside the shadow region and the number of pixels in the shadow region is at its maximum. The results are shown in Fig. 5(a) and (b). Fig. 5(a) shows the histogram of the original image and its shadow region, and Fig. 5(b) similarly shows the image of the second-order neighbor. Their gray levels range from 17 to 38 and 17 to 67, respectively. The highlight region is similarly manually selected from the histogram diagram when no noise pixels exist outside the highlight region and the number of pixels is at a maximum. Fig. 5(c) shows the histogram of the original image and its highlight region, and Fig. 5(d) shows the image for the second-order neighbor. The gray levels range from 219 to 225 and 195 to 255, respectively. In this case, the most pixels are observed when no noise is present.

Compared with Fig. 5(a) and (c), more pixels (or larger areas) are seen for the shadow and highlight regions in Fig. 5(b) and 5(d). The advantages of the GMRF model for local-texture features can be summarized as follows:

- (1) Some speckle noise is removed by the zero-mean Gaussian process.
- (2) For a sonar image, the MRF process can remove certain speckle noise, accentuate the shadow, and highlight regions over the sea-bottom reverberation region.

## 4. Level-set models with local texture features

### 4.1. Energy of the sonar image data

A sonar image has a limited number of structures to be segmented. In general, three classes of regions must be identified. We usually cannot expect uniformity in the intensity distribution probabilities of these three regions. The shadow region can be described by the Gaussian or Weibull law (Mignotte et al., 2000), the sea-bottom reverberation region by the Rayleigh or Weibull law (Mignotte et al., 2000), and, generally, the luminance within the highlight region, by a simple direct proportion law (Mignotte et al., 2000). However, the energy associated with the distribution probabilities in these three regions is not appropriate for segmenting unknown regions in a sonar image.

The energy under consideration here is associated with the local mean value by combining the original images with their local-texture feature data.

### 4.2. Variational level-set formulation of two-phase models

Let  $\Omega \in \mathbb{R}^2$  denote the image plane and let  $f : \Omega \times \mathbb{R} \rightarrow \mathbb{R}$  be a given sonar image. The energy associated with the local mean and

the length of contour  $C$  can be rewritten as

$$F(C, c_i, c_i^n) = \frac{1}{N+1} \left[ \sum_{i=1}^{N+1} \lambda_i \iint_{\Omega_i} (f - c_i)^2 dx dy + \sum_{n=1}^N \sum_{i=1}^2 \lambda_i^n \iint_{\Omega_i^n} (f^n - c_i^n)^2 dx dy \right] + \mu \cdot \text{length}(C) \quad (17)$$

where  $f$  is the original image, and  $f^n$  is the texture image in Eq. (10).  $N=5$  is the number of texture images. Eq. (17) is now written as

$$F(C, c_i, c_i^n) = \frac{1}{N+1} \sum_{n=1}^{N+1} \sum_{i=1}^2 \lambda_i^n \iint_{\Omega_i^n} (f^n - c_i^n)^2 dx dy + \mu \cdot \text{length}(C) \quad (18)$$

where  $c_i^n$  is the local intensity mean of  $f^n$  in  $\Omega_i^n$ ,  $\mu \geq 0$ ,  $\lambda_i^n > 0$ .

In the level-set formulation of moving fronts, active contours are represented by the zero level set  $C(t) = \{(x,y) | \phi(x,y,t) = 0\}$  of a level-set function  $\phi$ . We initialize  $\phi$  as a SDF (Sethian, 1999). Then, the energy,  $F(C, c_i^n)$ , can be written

$$F(\phi, c_1^n, c_2^n) = \mu \iint_{\Omega} |\nabla H(\phi)| dx dy + \frac{1}{N+1} \sum_{n=1}^{N+1} \left[ \lambda_1^n \iint_{\Omega^n} (f^n - c_1^n)^2 H(\phi) dx dy + \lambda_2^n \iint_{\Omega^n} (f^n - c_2^n)^2 (1 - H(\phi)) dx dy \right] \quad (19)$$

where  $H(\phi)$  is the Heaviside function.

Keeping  $\phi$  fixed and minimizing the energy  $F(\phi, c_1^n, c_2^n)$  in Eq. (19) with respect to the constants  $c_1^n$  and  $c_2^n$  yields the constant functions  $c_1^n$  and  $c_2^n$  with respect to  $\phi$

$$c_1^n(\phi) = \frac{\iint_{\Omega^n} f^n H(\phi) dx dy}{\iint_{\Omega^n} H(\phi) dx dy} \quad (20)$$

$$c_2^n(\phi) = \frac{\iint_{\Omega^n} f^n (1 - H(\phi)) dx dy}{\iint_{\Omega^n} (1 - H(\phi)) dx dy} \quad (21)$$

With  $c_1^n$  and  $c_2^n$  fixed and the energy  $F(\phi, c_1^n, c_2^n)$  minimized with respect to  $\phi$ , the evolution equation can be obtained by the Euler-Lagrange method and the Gauss' theorem as

$$\frac{\partial \phi}{\partial t} = \delta_\varepsilon(\phi) \left[ \mu \cdot \text{div} \left( \frac{\nabla \phi}{|\nabla \phi|} \right) + \frac{1}{N+1} \sum_{n=1}^{N+1} \left[ -\lambda_1^n (f^n - c_1^n)^2 + \lambda_2^n (f^n - c_2^n)^2 \right] \right] \quad (22)$$

To avoid re-initialization of the proposed model (Caselles et al., 1993, 1997; Sethian, 1999), we adopt the method used in Li et al. (2005) and write the evolution equation for Eq. (22) as

$$\frac{\partial \phi}{\partial t} = v \left[ \Delta \phi - \text{div} \left( \frac{\nabla \phi}{|\nabla \phi|} \right) \right] + \left\{ \delta_\varepsilon(\phi) \left[ \mu \cdot \text{div} \left( \frac{\nabla \phi}{|\nabla \phi|} \right) \right] \right\} \quad (23)$$

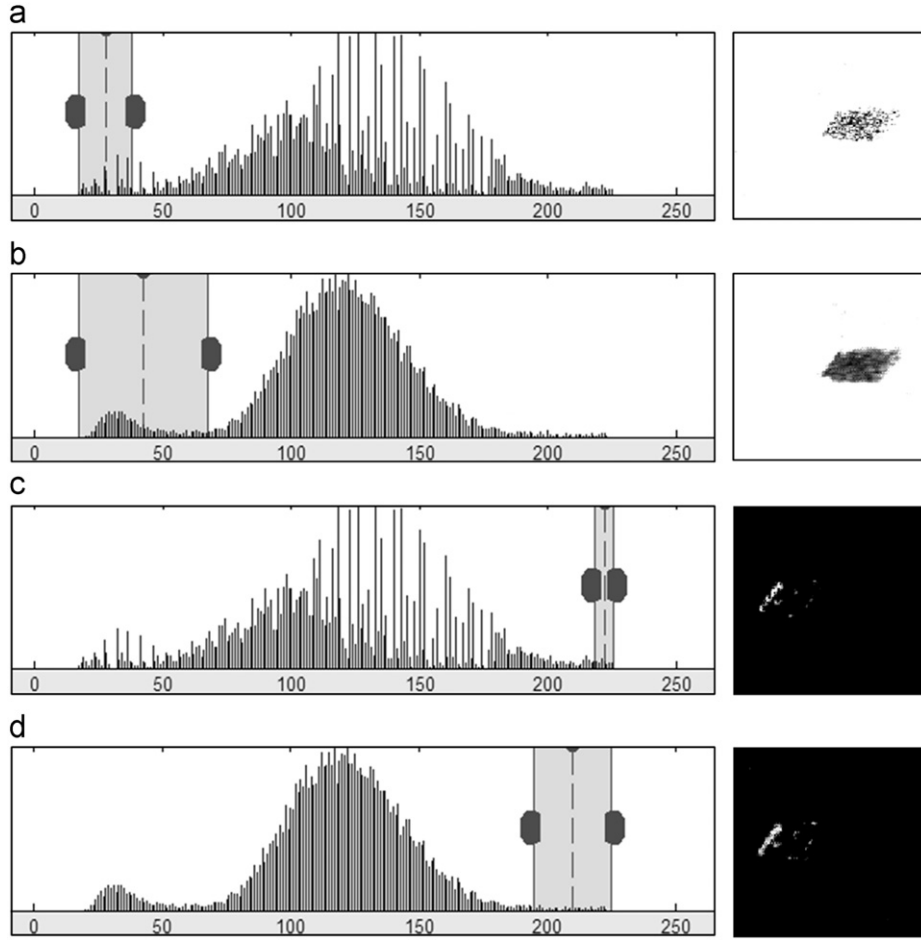


**Fig. 5.** The histograms of Fig. 4(a) and (c), and their shadow regions and highlight region that reserve the most pixels in present of no noise outside these regions: (a) The histogram of Fig. 4(a) and its shadow; (b) the histogram of Fig. 4(c) and its shadow; (c) the histogram of Fig. 4(a) and its highlight and (d) the histogram of Fig. 4(c) and its highlight.

$$+ \frac{1}{N+1} \sum_{n=1}^{N+1} \left[ -\lambda_1^n (f^n - c_1^n)^2 + \lambda_2^n (f^n - c_2^n)^2 \right] \quad (23)$$

where  $\nu > 0$ ,  $\Delta$  is the Laplacian operator, and  $\delta_\varepsilon(\phi)$  is the regularized Dirac function of Eq. (9).

The partial derivative,  $\partial\phi/\partial t$ , in Eq. (23) can be separated into two terms. The first is the internal energy of the function  $\phi$ , which drives  $\phi$  to keep a SDF (Li et al., 2005). The second term is the external energy of the function  $\phi$ , which drives the motion of the zero level curve of  $\phi$ . We can see that the second term contains the image information. Because the GMRF based texture image  $f^n$  reflects the spatial interaction in the image, it limits the speckle noise contained in the segmentation result. Interpreting  $c_i^n$  as the local or regional information of the image speeds up the movement of the zero level set  $\phi$  to the object. The contour or the edge information of the zero level curve  $\phi$  is then denoted as  $\text{div}(\nabla\phi/|\nabla\phi|)$ .

#### 4.3. Variational level-set formulation of multiphase models

In this section, we extend the two-phase model presented in Eq. (23) to a multiphase model. It is reasonable to assume that the four phases (or four classes) are reasonable to segment a sonar image.

Let  $\phi = (\phi_1, \phi_2)$ , where  $c^n = (c_{11}^n, c_{10}^n, c_{01}^n, c_{00}^n)$  is the local mean of each region shown in Fig. 1. The energy of four phases can be

written as

$$\begin{aligned} F(\phi, c^n) = & \mu \iint_{\Omega^n} |\nabla H(\phi_1)| dx dy + \mu \iint_{\Omega^n} |\nabla H(\phi_2)| dx dy + \frac{1}{N+1} \sum_{n=1}^N \\ & \times \left[ \lambda_1^n \iint_{\Omega^n} (f^n - c_{11}^n)^2 H(\phi_1) H(\phi_2) dx dy \right. \\ & + \lambda_2^n \iint_{\Omega^n} (f^n - c_{10}^n)^2 H(\phi_1) (1 - H(\phi_2)) dx dy \\ & + \lambda_3^n \iint_{\Omega^n} (f^n - c_{01}^n)^2 (1 - H(\phi_1)) H(\phi_2) dx dy \\ & \left. + \lambda_4^n \iint_{\Omega^n} (f^n - c_{00}^n)^2 (1 - H(\phi_1)) (1 - H(\phi_2)) dx dy \right] \end{aligned} \quad (24)$$

With  $\lambda_1^n = \lambda_2^n = \lambda_3^n = \lambda_4^n = \lambda^n$ , the Euler-Lagrange equations are obtained by minimizing Eq. (24) with respect to  $\phi$ . We then obtain

$$\begin{aligned} \frac{\partial\phi_1}{\partial t} = & \nu \left[ \Delta\phi_1 - \text{div} \left( \frac{\nabla\phi_1}{|\nabla\phi_1|} \right) \right] + \delta_\varepsilon(\phi_1) \left\{ \mu \cdot \text{div} \left( \frac{\nabla\phi_1}{|\nabla\phi_1|} \right) \right. \\ & \left. - \frac{1}{N+1} \sum_{n=1}^{N+1} \lambda^n [((f^n - c_{11}^n)^2 - (f^n - c_{01}^n)^2) H(\phi_2) + ((f^n - c_{10}^n)^2 \right. \\ & \left. - (f^n - c_{00}^n)^2) (1 - H(\phi_2))] \right\} \end{aligned} \quad (25)$$

$$\frac{\partial\phi_2}{\partial t} = \nu \left[ \Delta\phi_2 - \text{div} \left( \frac{\nabla\phi_2}{|\nabla\phi_2|} \right) \right] + \delta_\varepsilon(\phi_2) \left\{ \mu \cdot \text{div} \left( \frac{\nabla\phi_2}{|\nabla\phi_2|} \right) \right.$$

$$\left. \begin{aligned} & -\frac{1}{N+1} \sum_{n=1}^{N+1} \lambda^n [((f^n - c_{11}^n)^2 - (f^n - c_{01}^n)^2) H(\phi_1) \\ & + ((f^n - c_{10}^n)^2 - (f^n - c_{00}^n)^2)(1 - H(\phi_1))] \end{aligned} \right\} \quad (26)$$

where  $\nu > 0$ ,  $\mu \geq 0$ .

#### 4.4. Selection of the parameters

For the Chan–Vese two-phase model in Eq. (3), it is proper to discriminate the regions that have different intensity mean values for  $\lambda_1 = \lambda_2 = 1$ . Although many experiments have been performed to segment sonar images, it is more effective to segment the noisy sonar images when  $0.2 \leq \lambda_1 = \lambda_2 \leq 0.4$ . If the values of  $\lambda_1$  and  $\lambda_2$

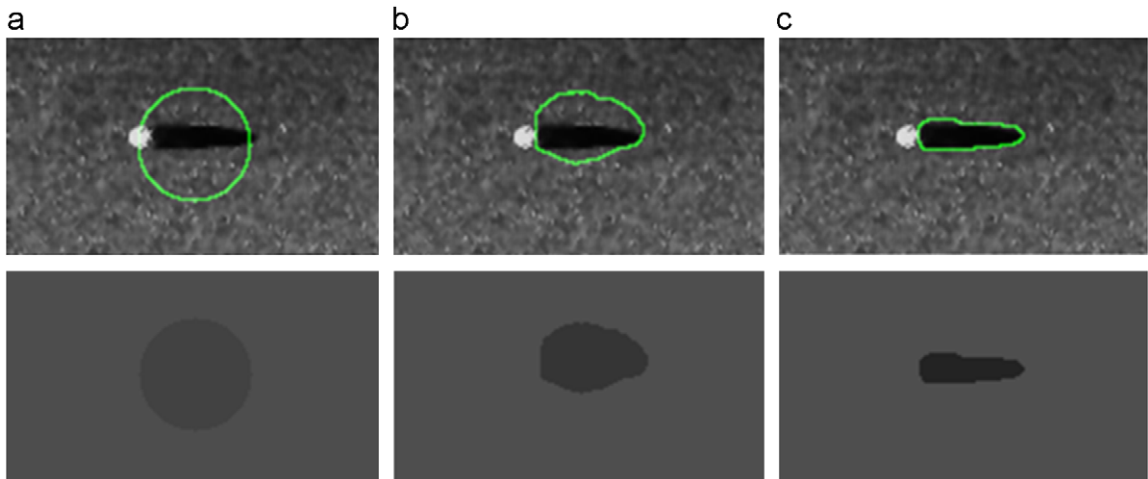


**Fig. 6.** Segmentation of a noisy synthetic sonar image (sized  $94 \times 161$ ) using the proposed two-phase model for iterative times of 80 and 200, respectively: (a) original synthetic sonar image and initial zero level set; (b) segmentation for iterative times of 80 and (c) segmentation for iterative times of 200.

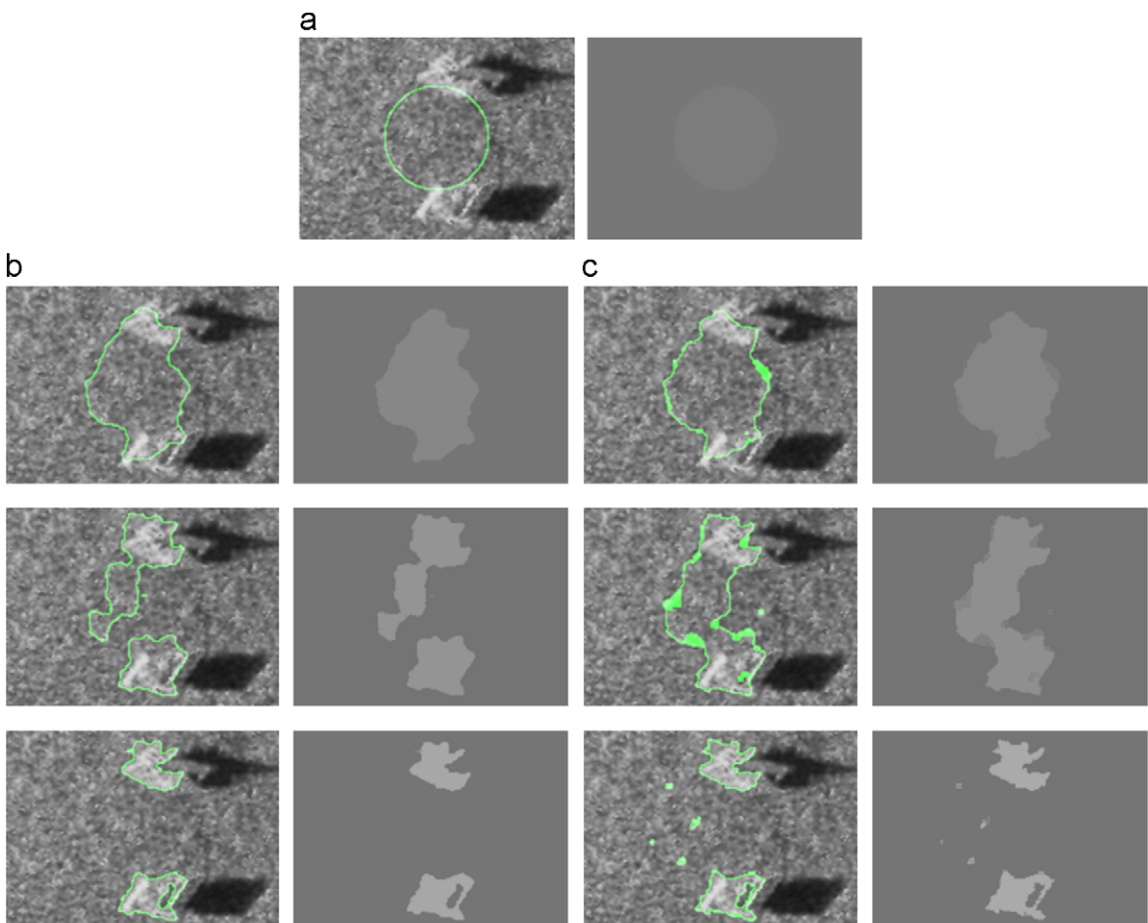


**Fig. 7.** Segmentation of a real sonar image (sized  $142 \times 191$ ) using two-phase model for iterative times of 120, 600 and 2000, respectively: (a) Original real sonar image and initial zero level set; (b) segmentation using the proposed two-phase model and (c) segmentation using Chan–Vese's two-phase model.

are too small, the zero level set  $\phi$  will be difficult to split and will move slowly; on the other hand, when their values are too large, the zero level set  $\phi$  will split too easily, resulting in segmentation results with too much noise.

In this paper,  $\lambda_1^n = \lambda_2^n = 0.2$  is used in the two-phase model of Eq. (23) and  $\lambda^n = 0.4$  in the multiphase model of Eqs. (25) and (26). The time step was set at  $\Delta t = 0.01$  and the space step at  $h = 1$  for  $v = 0.2/\Delta t$  and  $\mu = 0.01 \times 255^2$ .

The proposed models are suitable for sonar images that contain some highlighted and dark regions. The image can be partitioned into highlighted regions, dark regions, and others, but textures (such as sand ripples) cannot, as shown in Fig. 11, be segmented.

## 5. Experimental results

In this section, numerical examples are shown to validate the generality and effectiveness of the proposed models for both synthetic and real sonar image segmentations. The results were obtained using Matlab 7.4 with a 3.0 GHz Pentium processor and 1 GB of RAM.

One additional advantage of the developed model is that the model with the same set of parameters can work for a relatively wide range of different images, i.e., various sonar images can be segmented automatically using the same model. Because there is a significant amount of noise in sonar images, we used a Wiener

filter to reduce the noise contained in each image before the proposed methods and C-V methods are applied.

### 5.1. Segmentation results for the proposed two-phase model

Let  $widf$  and  $hei_f$  denote the width and height of an image. In the experiments, the initial level-set function  $\phi$  is chosen as a circle with its center at  $(widf/2, hei_f/2)$ . In the two-phase model, the radius is then selected from the smaller of  $widf/4$  and  $hei_f/4$ .

Our region of interest in a sonar image is the highlight or shadow area. It is desirable to first validate the proposed method on synthetic data in order to minimize the effect of other artifacts as much as possible. Fig. 6(a) is a synthetic sonar image modeled using the following models.

The noise model of the highlight can be represented as

$$Z_Y(y; r) = \frac{1}{r} \times (y - 155) \quad (27)$$

where  $\hat{r} = \sum_{i=1}^M (y_i - 155)$   $M$  is the number of the highlights, and  $y$  is the intensity.

The noise models of the shadow and reverberation are then described by the Weibull law

$$W_Y(y; \min, C, \alpha) = \frac{C}{\alpha} \left( \frac{(y - \min)}{\alpha} \right)^{C-1} \exp \left( - \left( \frac{(y - \min)}{\alpha} \right)^C \right) \quad (28)$$

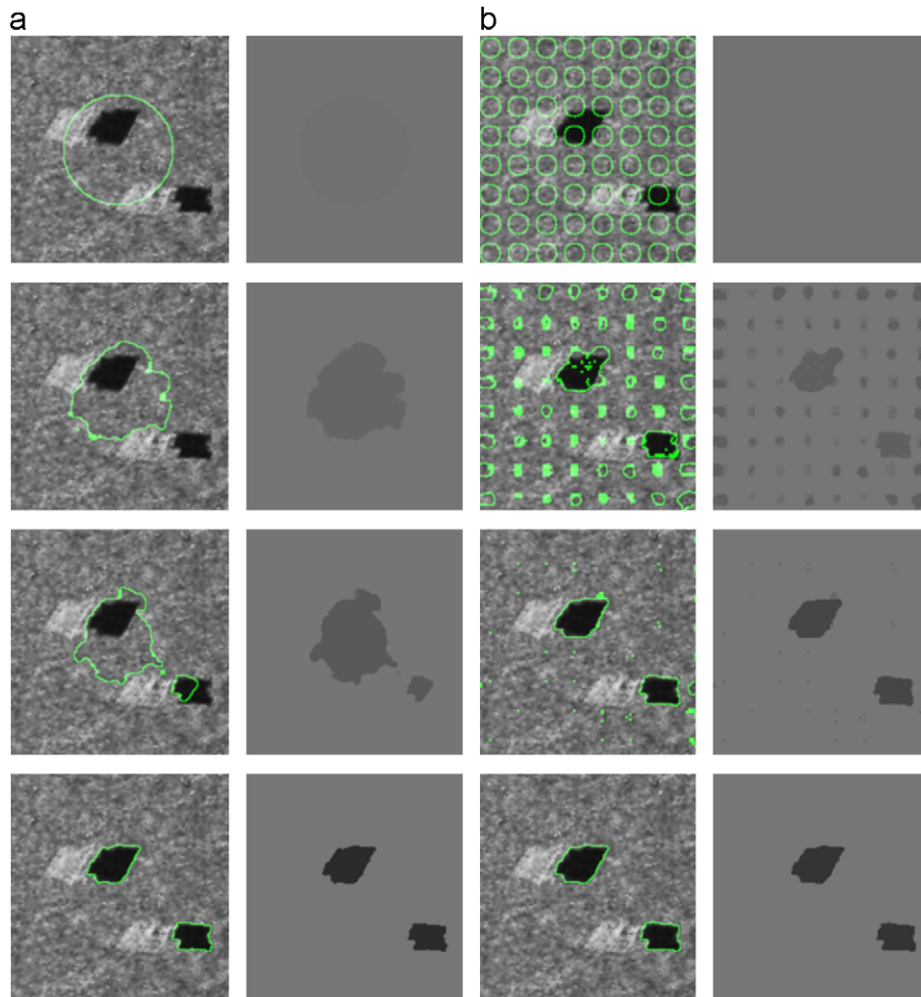


**Fig. 8.** Segmentation of a real sonar image (sized  $181 \times 172$ ) using the proposed two-phase model: (a) Initialization method of single circle and segmentation for iteration 40, 120 and 840, respectively and (b) initialization method of many small circles and segmentation for iteration 30, 80 and 200, respectively.

where  $\alpha$  and  $C$  are the scale and shape parameters, respectively

$$\widehat{m_{\min}} \approx \hat{y}_{\min} - 1, \frac{\sum_{i=1}^M (\hat{y}_i^{\hat{C}} \cdot \ln \hat{y}_i)}{\sum_{i=1}^M \hat{y}_i^{\hat{C}}} - \frac{1}{M} \sum_{i=1}^M \ln \hat{y}_i = \frac{1}{\hat{C}},$$

$$\hat{\alpha} = \left( \frac{1}{M} \sum_{i=1}^M \hat{y}_i^{\hat{C}} \right)^{1/\hat{C}}, \text{ and } \tilde{y}_i = (y_i - \widehat{m_{\min}}).$$

The average values for the highlight, shadow, and reverberation regions are 216, 9, and 78, respectively.

An example of the two-phase segmentation of a synthetic noisy sonar image with the model proposed in Eq. (23) is shown in Fig. 6. The iterative times of Fig. 6(b) and (c) are 80 and 200, respectively. This figure reveals nearly no noise in the results using the proposed two-phase model. The level set converges at iterative times of 200.

The segmentation results for a real sonar image are shown in Fig. 7. Two highlights and their respective shadows are presented. As can be seen, some parts of the boundaries of the two highlights are quite blurry. However, no speckle noise is present in the results using the proposed two-phase model, and the level set converges at iterative times of 2000. This can be compared with the Chan–Vese two-phase model, which requires greater iterative times for convergence and contains more noise in the segmentation results. Furthermore, in contrast to the Chan–Vese two-phase model, the proposed model contains the local-texture feature based on the GMRF of the image. Although the Chan–Vese two-phase model contains both the local and edge information of the objects, the local texture of the spatial interaction of the global image limits better the noise of the sonar image.

The segmentation results of another real sonar image using the proposed two-phase model are shown in Fig. 8. To reduce the

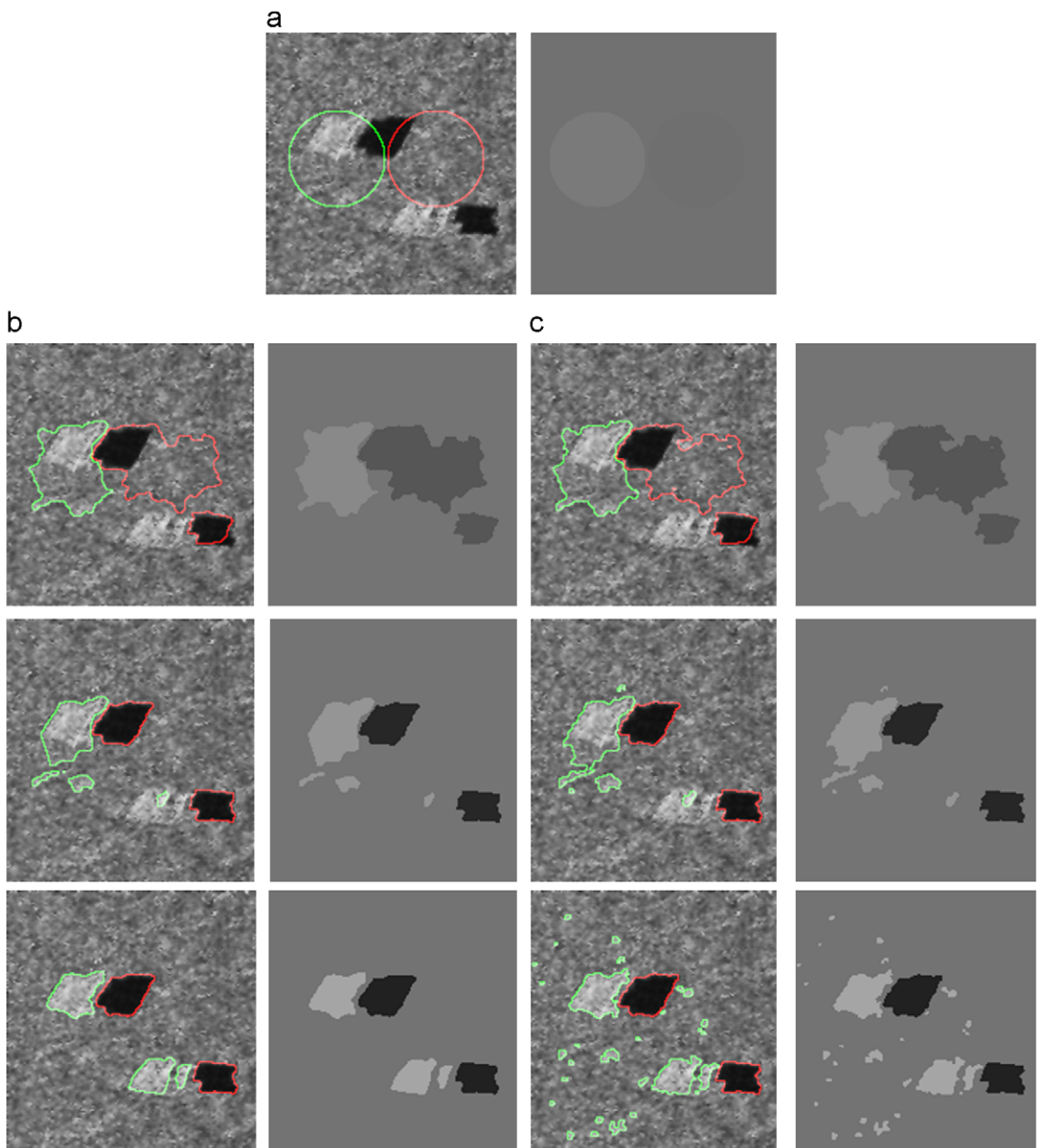


**Fig. 9.** Segmentation of a real sonar image (sized 181 × 172) using multiphase model for iterative times of 200, 800 and 3000, respectively: (a) original real sonar image and the initial zero level set; (b) segmentation using the proposed multiphase model and (c) segmentation using Vese–Chan's multiphase model.

iterative time, the level-set function  $\phi$  was initialized as many small circles, which results in global energy minimization in fewer iterations than observed in the single circle method. Furthermore, the shadow boundary was successfully extracted using the proposed two-phase model.

### 5.2. Segmentation results for the proposed multiphase model

This section presents the three-class segmentation results of the sonar images using Eqs. (25) and (26). To reduce the cost of computing the vacuum, two zero level sets of  $\phi_1$  and  $\phi_2$  with two circles, which are not intersected, were initiated. The abscissa of the center is  $widf/2$ , and the ordinate and radius are arbitrary.

The segmentation results using the proposed multiphase model on the image of Fig. 8 are shown in Fig. 9(b). We can see

that the intensities of the highlights are similar to those of some surrounding areas and that plentiful speckle noise is present in the sea-bottom reverberation region. The segmentation results using the proposed multiphase model are robust and converge after 3000 times of iteration, in contrast to the noisier results using the Chan-Vese multiphase model, which requires further iteration as well; see Fig. 9(c).

As depicted in Fig. 10(a), although three irregular highlights lie together, excellent contours are still obtained with the proposed multiphase model for different initialization methods, despite the presence of strong speckle noise; see Figs. 10(c) and (d). Convergence occurred after 1400 and 800 iterations, respectively.

Seabed segmentation results are shown in Fig. 11. These results show that the proposed multiphase model performs robustly even there are no clear boundaries for noisy seabeds.

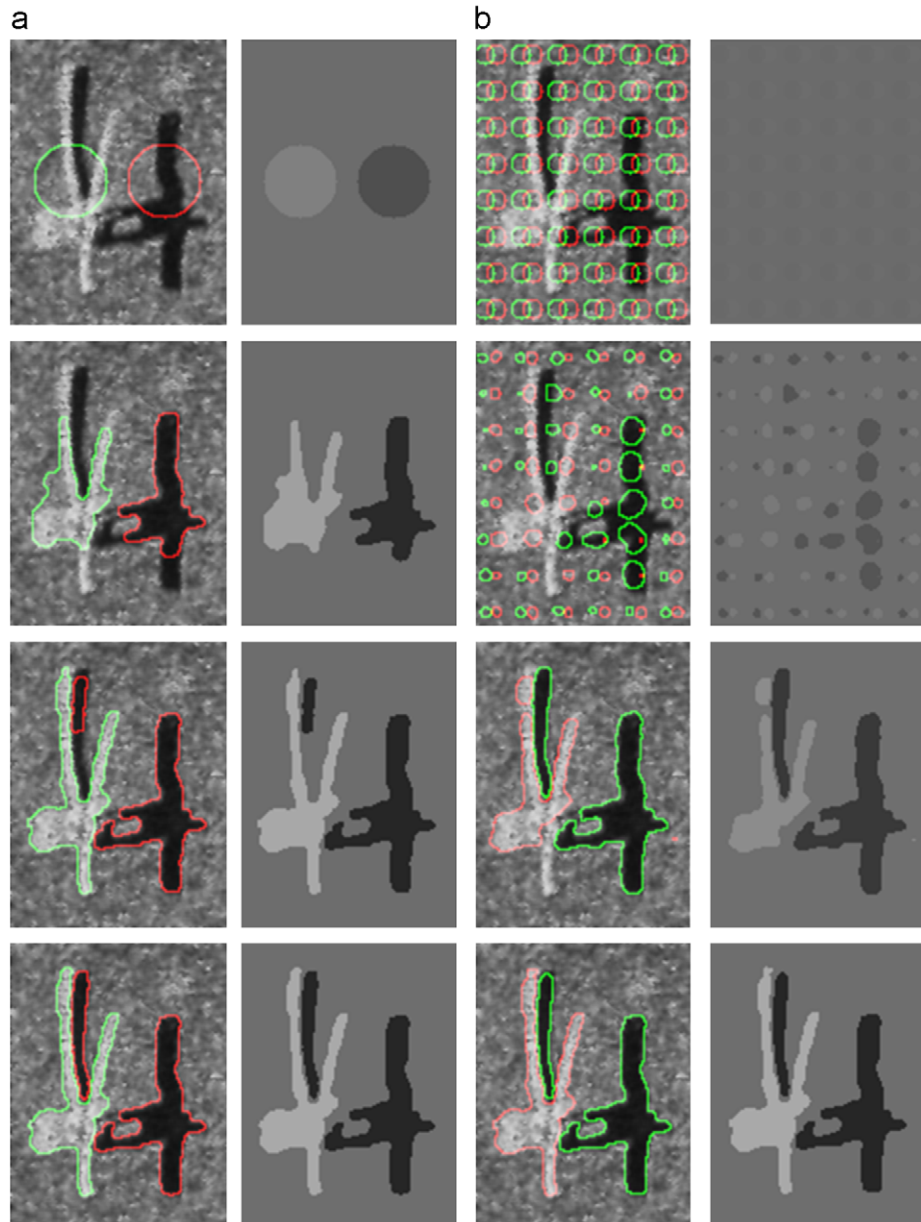


**Fig. 10.** Segmentation of a real sonar image (sized  $151 \times 115$ ) using the proposed multiphase model: (a) Initialization method of single circle and segmentation for iteration 100, 1200 and 1400, respectively and (b) initialization method of many small circles and segmentation for iteration 40, 120 and 800, respectively.

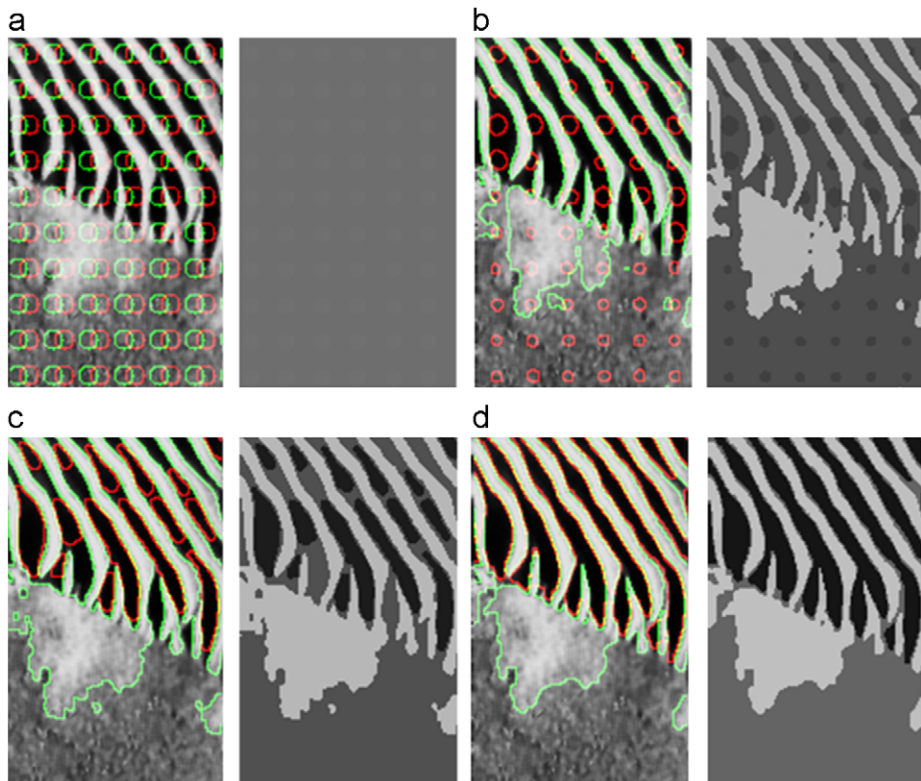


**Fig. 11.** Segmentation of a real sonar image of seabed (sized  $187 \times 116$ ) using multiphase model: (a) Original real sonar image of seabed and initialization method of many small circles and (b) segmentation for iteration 30; (c) segmentation for iteration 80 and (d) segmentation for iteration 360.

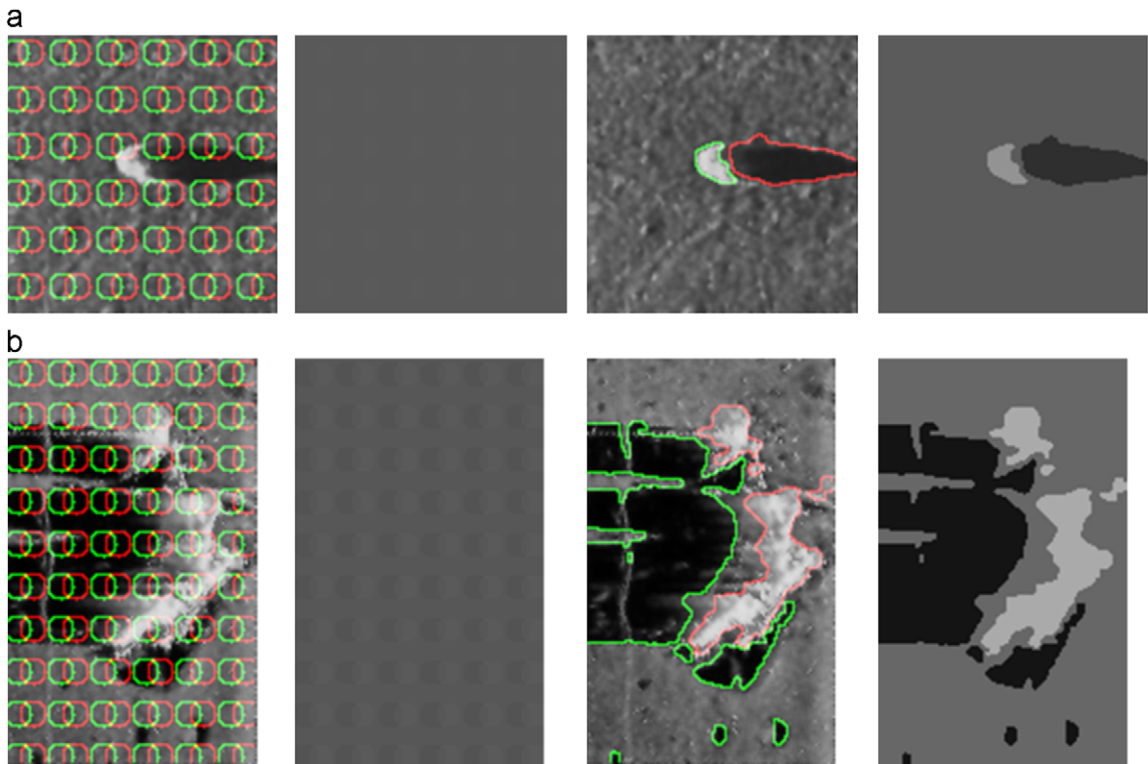


**Fig. 12.** Segmentation of a real sonar image of rocks using multiphase model: (a) A starboard sonar image (sized  $133 \times 129$ ) including a rock and its segmentation for iteration 720 and (b) A larboard sonar image (sized  $193 \times 118$ ) including rocks, which are buried partly in the sand and their segmentation for iteration 840.

Finally, the segmentation results of images with some rocks are presented in Fig. 12. Fig. 12(a) shows a starboard sonar image with a rock and its segmentation results after 720 iterations. Fig. 12(b)

shows a larboard sonar image with rocks, which are partly buried in the sand, and their segmentation results after 840 iterations. These results show that the proposed multiphase model can obtain

better segmentation results regardless of the types of sonar or the relative positions of the highlight and shadow regions.

## 6. Conclusions

We have presented two new level-set models for the segmentation of sonar images. Their effectiveness was verified through a number of experiments on real sonar images. The texture images extracted by the GMRF model were combined into the proposed level-set models, which contain the spatial interaction, global, local, and edge information of the objects. Thus, these methods can improve the segmentation of sonar images with severe speckle noise. The experiments showed that the proposed models achieve relatively accurate and robust results for various sonar images without clear object boundaries at a wide range of noise levels. The proposed models can segment a noisy sonar image into two or more regions without re-initialization and can be extended to other similar applications where the images are severely corrupted by noise.

## Acknowledgements

The authors thank LAUREL TECNOLOGIES in Beijing for providing numerous real sonar pictures. Sonar images in Fig. 11 and Fig. 12(b) are derived from the Internet, and the IP addresses are '<http://www.marinesonic.us/archives.php>' and '<http://www.digitaljournal.com/image/49037>', respectively. The authors thank the providers for these images.

## References

- Brox, T., Weickert, J., 2006. Level set segmentation with multiple regions. *IEEE Transactions on Image Processing* 15 (10), 3213–3218.
- Caselles, V., Catte, F., Coll, T., Dibos, F., 1993. A geometric model for active contours in image processing. *Numerische Mathematik* 66 (1), 1–31.
- Caselles, V., Kimmel, R., Sapiro, G., 1997. Geodesic active contours. *International Journal of Computer Vision* 22 (1), 61–79.
- Chan, T.F., Vese, L.A., 2001. Active contours without edges. *IEEE Transactions on Image Processing* 10 (2), 266–277.
- Chung, G., Vese, L.A., 2005. Energy minimization based segmentation and denoising using a multilayer level set approach. In: Proceedings of the Fifth International Workshop on Energy Minimization Methods in Computer Vision and Pattern Recognition, IAPR, Florida, USA, Vol. 3757, pp. 439–455.
- Haralick, R.M., Shanmugam, K., Dinstein, I., 1973. Textural features for images classification. *IEEE Transactions on Systems, Man, and Cybernetics* 3 (6), 610–621.
- Krishnamachari, S., Chellappa, R., 1997. Multiresolution Gauss–Markov random field models for texture segmentation. *IEEE Transactions on Image Processing* 6 (2), 251–267.
- Lianantonakis, M., Petillot, Y.R., 2005. Sidescan sonar segmentation using active contours and level set methods. *Oceans-Europe, OE, Brest, France* 1, 719–724.
- Lianantonakis, M., Petillot, Y.R., 2007. Sidescan sonar segmentation using texture descriptors and active contours. *IEEE Journal of Oceanic Engineering* 32 (3), 744–752.
- Li, C., Xu, C., Gui, C., Martin, D., 2005. Level set evolution without re-initialization: a new variational formulation. *Proceedings of the IEEE Computer Society Conference on Computer Vision and Pattern Recognition, CA, San Diego, USA* 1, 430–436.
- Mansouri, A.R., Mitiche, A., Vazquez, C., 2006. Multiregion competition: a level set extension of region competition to multiple region image partitioning. *Computer Vision and Image Understanding* 101 (3), 137–150.
- Mignotte, M., Collet, C., 1999. Three-class Markovian segmentation of high-resolution sonar images. *Computer Vision and Image Understanding* 76 (3), 191–204.
- Mignotte, M., Collet, C., Pérez, P., Bouthemy, P., 2000. Sonar image segmentation using an unsupervised hierarchical MRF model. *IEEE Transactions on Image Processing* 9 (7), 1216–1231.
- Mumford, D., Shah, J., 1989. Optimal approximation by piecewise smooth functions and associated variational problems. *Communications on Pure and Applied Mathematics* 42, 577–685.
- Osher, S., Sethian, J.A., 1988. Fronts propagating with curvature dependent speed: algorithms based on Hamilton–Jacobi formulations. *Journal of Computational Physics* 79, 12–49.
- Reed, S., Petillot, Y., Bell, J., 2003. An automatic approach to the detection and extraction of mine features in sidescan sonar. *IEEE Journal of Oceanic Engineering* 28 (1), 90–105.
- Schmitt, F., Mignotte, M., Collet, C., Thourel, P., 1996. Estimation of noise parameters on sonar images. *Proceedings of SPIE—the International Society for Optical Engineering, SPIE, Washington, USA* 2823, 2–12.
- Sethian, J.A., 1999. *Level Set Methods and Fast Marching Methods*. Cambridge University Press, Cambridge.
- Vese, L.A., Chan, T.F., 2002. A multiphase level set framework for image segmentation using the Mumford and Shah model. *International Journal of Computer Vision* 50 (3), 271–293.